Available online at www.sciencedirect.com

SciVerse ScienceDirect

Ceramics International 39 (2013) 389–394

CERAMICS INTERNATIONAL

www.elsevier.com/locate/ceramint

Electrochemical performance of $Ni_{1-x}Fe_x$–$Ce_{0.8}Gd_{0.2}O_{1.9}$ cermet anodes for solid oxide fuel cells using hydrocarbon fuel

Chun-Kang Cho[a], Byung-Hyun Choi[b], Ki-Tae Lee[a,c,*]

[a]Division of Advanced Materials Engineering, Chonbuk National University, Jeonbuk 561-756. Republic of Korea
[b]Optic and Electronic Ceramics Division, Korea Institute of Ceramic Engineering and Technology, Seoul 153-801, Republic of Korea
[c]Hydrogen and Fuel Cell Research Center, Chonbuk National University, Jeonbuk 561-756, Republic of Korea

Received 28 May 2012; received in revised form 13 June 2012; accepted 13 June 2012
Available online 19 June 2012

Abstract

$Ni_{1-x}Fe_x$ bimetallic-based cermet anodes were investigated for hydrocarbon-fueled solid oxide fuel cells. $Ni_{1-x}Fe_x$–$Ce_{0.8}Gd_{0.2}O_{1.9}$ cermet anodes were synthesized using a glycine nitrate process, and their electrical conductivity and the amount of carbon deposits were found to decrease with increasing Fe content. The anode polarization resistance for the CH_4 fuel was significantly reduced by Fe alloying, which was strongly related to the carbon deposition behavior. The maximum power density of the single cell with $Ni_{0.85}Fe_{0.15}$–$Ce_{0.8}Gd_{0.2}O_{1.9}$ in CH_4 at 800 °C was 0.27 W/cm^2. Fe alloying significantly improved the electrochemical performance of solid oxide fuel cells in CH_4 fuel by suppressing carbon deposition.

Keywords: E Solid oxide fuel cell; E Cermet anode; C Electrical conductivity; Carbon deposition

1. Introduction

A major advantage of solid oxide fuel cells (SOFCs) is the fuel flexibility in that hydrocarbon fuels such as CH_4 can be used directly via an internal reforming process instead of pure hydrogen fuel [1–3]. This is feasible due to the high operating temperature of SOFCs. The state-of-the-art anode material for SOFCs is nickel-yttria stabilized zirconia (Ni-YSZ) cermet [1]. Although nickel shows superior catalytic activity for hydrogen oxidation, when hydrocarbon fuel is used as a fuel, the formed carbon can be deposited on the Ni surface, which can result in performance degradation [4,5]. Nickel is well known as a catalyst for the growth of carbon nanotubes or fibers [6,7].

There have been various investigations of novel anode materials to overcome the carbon deposition problem, such as ceria-based and perovskite oxides [8–10]. To decrease carbon deposition, Ni in the Ni-YSZ cermet anode can be partly or completely replaced by other metals, such as Co or Cu. Itome and Nelson demonstrated that the rate of methane conversion with Co-YSZ cermet increased at high temperatures [11]. Additionally, Cu exhibited tolerance for carbon deposition when a hydrocarbon fuel was used [12]. Ceria (CeO_2)-based catalysts are used to suppress coking or desulfurization in catalytic processes and have a high catalytic activity for methane oxidation [13]. Ingram and Linic reported that the calculated activity of Fe in the direct utilization of hydrocarbon fuels under SOFC operating conditions was comparable to that of Ru and Ni [14]. With the exception of a few studies of Ni–Fe based anodes, a systematic investigation of the factors that control their carbon deposition behavior and electrocatalytic activity is scarcely available in the literature [15–17]. With this perspective, in this paper we present the effects of Fe alloying on crystal chemistry, electrical conductivity, carbon deposition, and electrochemical performance based on the carbon deposition behavior.

2. Experimental procedure

$Ni_{1-x}Fe_xO$-GDC powders ($x=0$, 0.05, 0.1, 0.15) were synthesized by a glycine nitrate process (GNP). An

*Corresponding author at: Chonbuk Natioanl University, Division of Advanced Materials Engineering, 664-14 Deokjin-dong 1ga, Deokjin-gu, Jeonbuk 561-756, Republic of Korea. Tel.: +82 63 270 2290; fax: +82 63 270 2386.
E-mail address: ktlee71@jbnu.ac.kr (K.-T. Lee).

0272-8842/$36.00
http://dx.doi.org/10.1016/j.ceramint.2012.06.039

appropriate amount of $Ni(NO_3)_2 \cdot 6H_2O$ (Alfa Aesar, 98%), $Fe(NO_3)_3 \cdot 9H_2O$ (Alfa Aesar, 98%), $Ce(NO_3)_3 \cdot 6H_2O$ (Aldrich, 99% metal basis), $Gd(NO_3)_3 \cdot 6H_2O$ (Alfa Aesar, 99.9%, REO), and glycine (Alfa Aesar, 99%) were dissolved in deionized water. After stirring for 2 h, the mixed solution was heated at approximately 250 °C until combustion occurred. The ashes formed by combustion were calcined at 750 °C for 2 h. After ball-milling with zirconia balls for 24 h, the synthesized $Ni_{1-x}Fe_xO$-GDC powders were reduced to $Ni_{1-x}Fe_x$-GDC in H_2 at 800 °C for 2 h. The $Ni_{1-x}Fe_x$-GDC composites were synthesized at a mixing ratio of 60:40 vol%.

Phase analysis was performed by X-ray diffraction using an X-ray diffractometer (Rigaku Model D/MAX-111A, Japan) with Cu K_α radiation. Diffraction patterns were recorded at a scan rate of 4°/min in a 2θ range of 20° to 60°. Lattice constants were calculated from the XRD results. For the microstructure analysis and electrical conductivity measurements, bar-type samples were fabricated by sintering in an air atmosphere at 1400 °C for 4 h. The microstructure and composition of the samples were confirmed by scanning electron microscopy/energy-dispersive X-ray spectroscopy (SEM/EDX, SN-3000 Hitachi, Japan). The electrical conductivity and porosity of the sintered samples were measured by the DC four-probe method and a mercury porosimeter (UPA-150, Microtrac, USA), respectively. The amount of carbon deposits was calculated by thermal gravimetric analysis (TGA, TA Q600, TA Instruments Ltd., USA). After the calcined samples were exposed to a dry CH_4 atmosphere at 800 °C for 3 h, TGA was then executed from room temperature to 900 °C at a heating rate of 20 °C/min in air, allowing the deposited carbon to re-oxidize with oxygen. The amount of deposited carbon was calculated by analyzing the weight loss from 500 to 700 °C.

Symmetrical half-cells with 8YSZ electrolyte were fabricated for electrochemical characterization. 8YSZ pellets were sintered with commercial YSZ powder (TZ-8YSZ, Tosoh, Japan) at 1450 °C for 4 h. The $Ni_{1-x}Fe_xO$-GDC anode paste was prepared by mixing the anode powder and binder (Heraeus V006) at a ratio of 70:30 wt%, and the paste was screen-printed on both sides of the YSZ pellet. Both electrodes were fired at 1250 °C for 2 h. The geometrical area of the electrode was 0.25 cm^2. Pt mesh and Pt wire were used as the current collector and lead, respectively. AC impedance measurements for the symmetric cells were performed using a potentiostat (SP150, Biologic SAS, France) equipped with a frequency response analyzer under open-circuit conditions at 800 °C in H_2 and CH_4 atmospheres. The applied frequency ranged from 50 μHz to 100 kHz with a voltage amplitude of 20 mV. Current–voltage (I–V) measurements of single cells with a $Ba_{0.5}Sr_{0.5}Co_{0.8}Fe_{0.2}O_{3-\delta}$–$Ce_{0.8}Gd_{0.2}O_{1.9}$ (BSCF-GDC) cathode and YSZ electrolyte were performed.

A $Ni_{1-x}Fe_x$-GDC ($x=0$, 0.15) cermet anode layer was screen-printed onto 0.3-mm thick YSZ pellets and then fired at 1250 °C for 2 h. Similarly, the BSCF-GDC cathode layer was screen-printed onto the other side of the YSZ pellets in a symmetric position, followed by firing at 1050 °C for 2 h. The geometric area of both electrodes was 0.25 cm^2. A Pt mesh pushed onto the electrode with a spring loaded alumina tube was used as the current corrector. A seal between the single cell and alumina tube was achieved with a Pyrex® glass ring. Humidified H_2 (~3% H_2O at 30 °C) and air were supplied as the fuel and oxidant, respectively, at a rate of 100 cm^3/min. Humidified CH_4 was also used as the fuel to verify the hydrocarbon fuel use.

3. Results and discussion

The X-ray diffraction patterns of the $Ni_{1-x}Fe_xO$-GDC powders ($x=0$, 0.05, 0.1, 0.15) calcined at 750 °C for 2 h are shown in Fig. 1(a). Peaks of Fe_2O_3 were observed when Fe was added to NiO, indicating that Fe is not soluble in NiO. However, when the calcined samples were reduced in

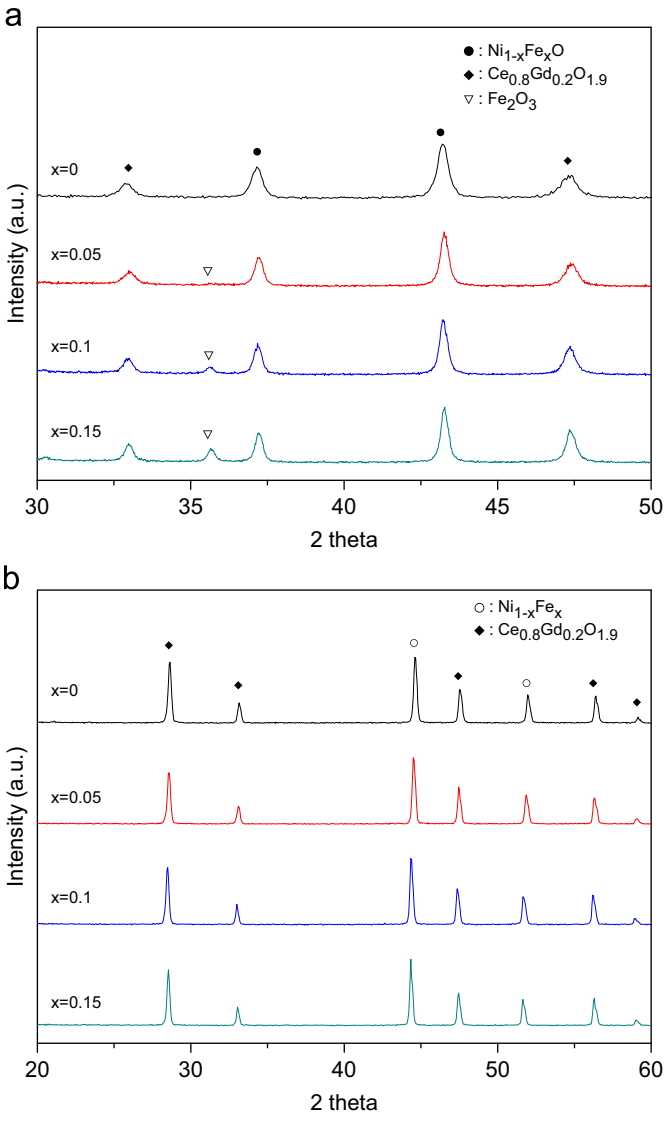

Fig. 1. XRD patterns of the $Ni_{1-x}Fe_xO$-GDC composites (a) calcined in air at 750 °C for 2 h and (b) reduced in H_2 at 800 °C for 2 h.

the H_2 atmosphere at 800° C for 2 h, Fe was completely alloyed in the Ni lattice in $Ni_{1-x}Fe_x$-GDC, as shown in Fig. 1(b). The Ni peaks shifted toward low 2θ as the Fe content increased. This shift is attributed to an increase in the lattice constant of Ni caused by Fe alloying and is primarily due to the difference in atomic radii of Ni (R_{Ni}=1.24 Å) and Fe (R_{Fe}=1.72 Å) [18]. Meanwhile, the reduction of Fe_2O_3 to Fe is thermodynamically feasible in the H_2 atmosphere at 800 °C. It has been reported that Fe_2O_3 was reduced to Fe in H_2 below 600 °C [19,20].

Quantitative analysis of the synthesized samples was performed using EDX to verify the designed compositions and the results are listed in Table 1. Based on the elemental analysis, the synthesized samples had the expected stoichiometries.

The geometrical morphology of the samples should be considered as the electrical conductivity strongly depends on the microstructure. Fig. 2 shows the microstructures of the reduced samples after sintering at 1400 °C for 4 h in air and the measured porosity of the samples is listed in Table 2. Although no pore formers were used, all samples had a porous structure. In general, pores in Ni-based cermet anodes without pore formers are derived from two sources; incomplete sintering and the reduction of NiO. The porosity and average pore size of the $Ni_{1-x}Fe_x$-GDC samples increased slightly with increasing Fe content. However, there was no significant change in the porous microstructure.

The electrical conductivities of the $Ni_{1-x}Fe_x$-GDC samples measured by the DC 4-probe method are shown in Fig. 3. The electrical conductivity of the samples decreased with increasing Fe content. Similarly, the electrical resistivities of electrodeposited Ni–Fe alloys increased monotonically with increasing Fe content [21,22]. This electrical behavior of the Ni–Fe bimetallic system is due to the enhancement of electron scattering caused by the solid solution effect based on Nordheim's rule. Additionally, the resistivity of Ni–Cu and Ni–Co alloys increases with Cu and Co content, respectively, which means the electrical conductivity decreases [23,24].

The calculated carbon deposition rates of all the samples from the TGA data are shown in Fig. 4. The amount of carbon deposits significantly decreased with Fe alloying. The formation of carbon at CH_4 fueled-SOFC anodes

Table 1
EDX elemental analysis data for the synthesized $Ni_{1-x}Fe_x$-GDC samples.

Composition	Element stoichiometry (molar ratio)			
	Ni/(Ni+Fe)	Fe/(Ni+Fe)	Ce/(Ce+Gd)	Gd/(Ce+Gd)
x=0	1	0	0.793	0.207
x=0.05	0.951	0.049	0.795	0.205
x=0.1	0.908	0.092	0.805	0.195
x=0.15	0.852	0.148	0.810	0.190

Table 2
Porosity and average pore size of the $Ni_{1-x}Fe_x$-GDC cermet anode materials reduced at 800 °C for 2 h in H_2.

Composition	Porosity (%)	Average pore size (nm)
x=0	32	175
x=0.05	34	186
x=0.1	36	193
x=0.15	36	197

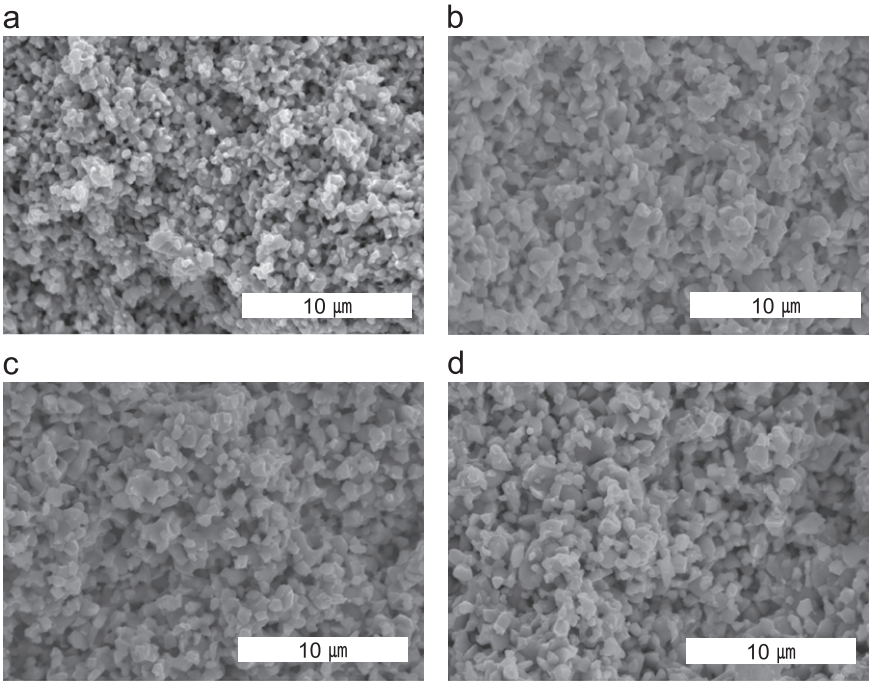

Fig. 2. Cross-sectional SEM micrographs of $Ni_{1-x}Fe_x$-GDC cermets reduced in H_2 at 800 °C for 2 h after sintering at 1400 °C for 4 h in air: (a) x=0, (b) x=0.05 (c) x=0.1 and (d) x=0.15.

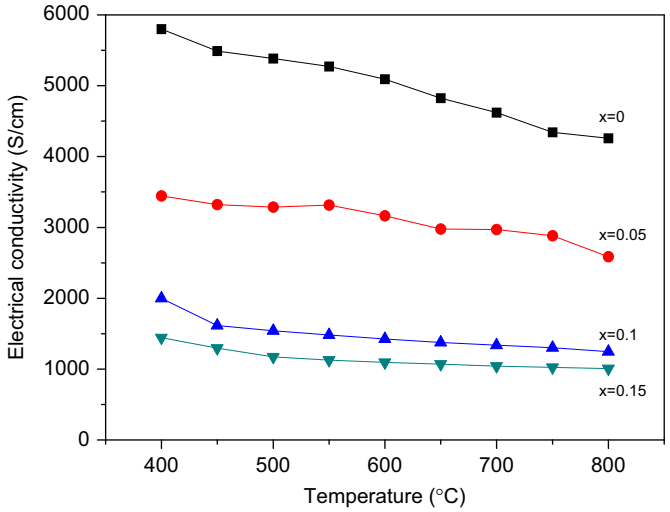

Fig. 3. Electrical conductivity of the $Ni_{1-x}Fe_x$-GDC cermets measured in a reducing atmosphere.

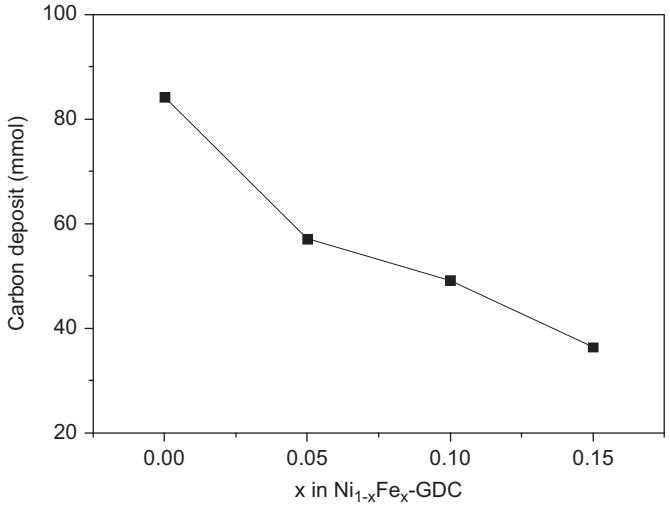

Fig. 4. Carbon deposition rate of the $Ni_{1-x}Fe_x$-GDC cermets with various Fe contents.

generally occurs via pyrolysis ($CH_4 \rightarrow C + 2H_2$) or the Boudouard reaction ($2CO \rightarrow CO_2 + C$). In the Boudouard reaction, CO can be supplied by a steam reforming process ($CH_4 + H_2O \rightarrow CO + 3H_2$) or partial oxidation reaction ($CH_4 + O^{2-} \rightarrow CO + 2H_2 + 2e^-$). However, in this study, carbon deposits primarily originated from CH_4 pyrolysis because the carbon deposition behavior was evaluated in a dry CH_4 atmosphere. Both carbon filaments and nickel carbides from the cracked carbon species are easily formed on Ni surfaces [25,26]. Nikolla et al. reported that Sn-containing surface alloys can suppress the formation of C–C bonds and/or have a lower thermodynamic driving force for carbon nucleation on low-coordinated sites [27]. Similarly, Fe alloying in a Ni matrix could suppress carbon deposition by breaking up ensembles of Ni atoms, which are required for the sustained growth of solid carbon deposits.

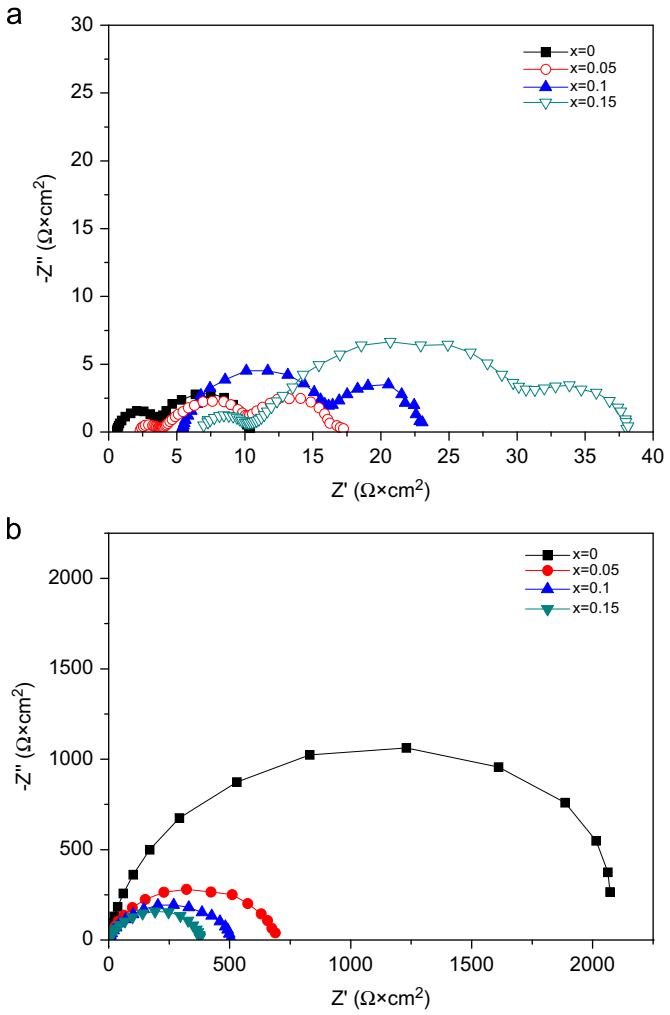

Fig. 5. Typical AC impedance spectra of symmetrical half-cells with a $Ni_{1-x}Fe_x$-GDC cermet anode and YSZ electrolyte in (a) H_2 and (b) CH_4 at 800 °C.

Typical AC impedance spectra of the symmetrical half-cells with an YSZ electrolyte at 800 °C are shown in Fig. 5. Considering the oxidation of H_2 via the CH_4 cracking process, the H_2-fueled SOFCs would be expected to exhibit better electrochemical performance than CH_4-fueled SOFCs. The anode polarizations of all samples for CH_4 fuel were much greater than for H_2 fuel due to the lower concentration of H_2 and slower pore diffusion of CH_4 molecules than H_2 molecules due to the larger size.

Variations in the calculated R_p values from the AC impedance data measured in H_2 and CH_4 atmospheres are shown in Fig. 6. The R_p value increased with increasing Fe content in the H_2 atmosphere, but decreased in the CH_4 atmosphere. The anode reaction on the SOFC is generally considered to be multiphase, including catalytic activation, adsorption/dissociation of the hydrogen molecule, charge transfer, and gas diffusion. Both the electrical conductivity and catalytic activity of the anode material are critical for maximizing electrochemical performance in an H_2 atmosphere. Reduced electrical conductivity by Fe alloying inhibits the charge transfer reaction due to the lack of electrons and

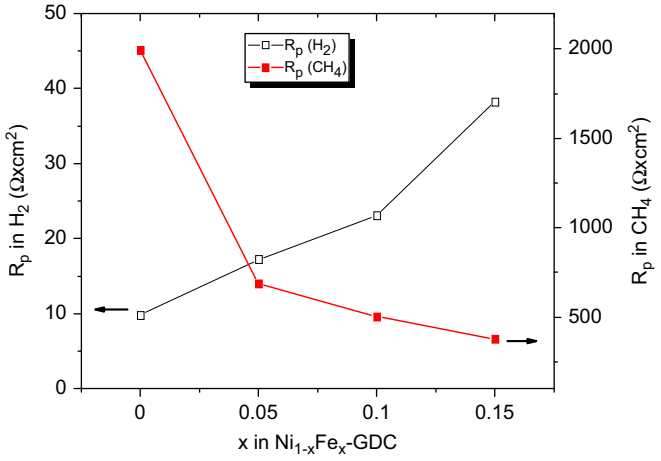

Fig. 6. Variation in R_p values of the $Ni_{1-x}Fe_x$-GDC cermets with various Fe contents in H_2 and CH_4 at 800 °C.

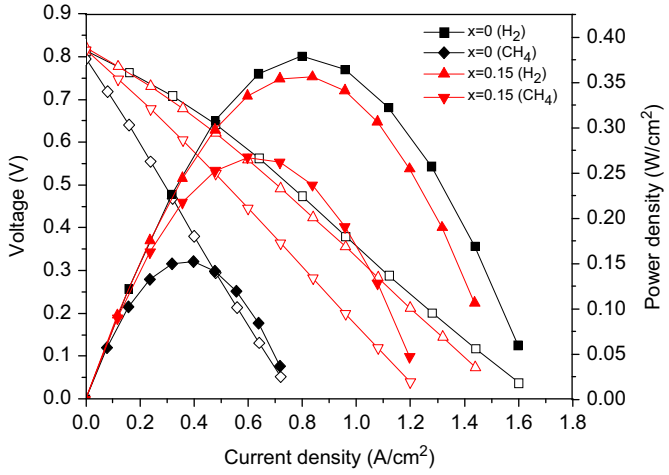

Fig. 7. Comparison of the *I–V* curves and power densities of the $Ni_{1-x}Fe_x$-GDC (x=0, 0,15) cermet anodes at 800 °C.

decreased number of reaction sites due to the disruption of Ni atom ensembles by Fe atoms, leading to a decrease in catalytic activity. Consequently, the electrochemical performance in the H_2 atmosphere degrades with Fe alloying. Alternatively, the gas diffusion may be the rate-determining step for the anode reaction in the CH_4 atmosphere because the deposited carbons block the anode pores. Moreover, the deposited carbons may cover the reaction sites, leading to a decrease in catalytic activity. The variation in the R_p values in the CH_4 atmosphere showed the same trends observed for the carbon deposition rate, as shown in Fig. 4. Consequently, Fe alloying could suppress carbon deposition, leading to a decrease in anode polarization for the CH_4 fuel.

Fig. 7 compares the *I–V* curves and power density of the Ni-GDC and $Ni_{0.85}Fe_{0.15}$-GDC anodes at 800 °C. While the $Ni_{0.85}Fe_{0.15}$-GDC anode showed slightly poorer performance than the Ni-GDC anode in H_2, the single cell with the $Ni_{0.85}Fe_{0.15}$-GDC anode showed significantly better electrochemical performance in the CH_4 fuel than the Ni-GDC anode. The maximum power densities of the single cells with Ni-GDC and $Ni_{0.85}Fe_{0.15}$-GDC in CH_4 at 800 °C were 0.15 W/cm^2 and 0 27 W/cm^2, respectively.

4. Conclusions

$Ni_{1-x}Fe_x$ bimetallic-based cermets were investigated as alternative SOFC anode materials for hydrocarbon fuel use. The electrical conductivity of the $Ni_{1-x}Fe_x$-GDC cermets decreased with increasing Fe content. The carbon deposition rate decreased with Fe alloying due to suppression of C–C bond formation and/or lowering of the thermodynamic driving force for carbon nucleation. The anode polarization resistance in the CH_4 atmosphere also decreased with increasing Fe content. The electrochemical performance of the $Ni_{1-x}Fe_x$-GDC cermet anode materials in the CH_4 fuel was strongly correlated with the carbon deposition behavior. Consequently, Fe alloying was effective in suppressing carbon deposition and improving the electrochemical performance of the CH_4-fueled SOFCs.

Acknowledgements

This work was supported by a New & Renewable Energy grant from the Korea Institute of Energy Technology Evaluation and Planning (KETEP) funded by the Korean Ministry of Knowledge Economy (2010T100100622). This work was also supported by the Human Resources Development of the Korea Institute of Energy Technology Evaluation and Planning (KETEP) funded by the Korean government through the Ministry of Knowledge Economy (Grant No. 20114030200060).

References

[1] N.Q. Mihn, Ceramic fuel cells, Journal of the American Ceramic Society 76 (1993) 563–588.
[2] S.P. Jiang, S.H. Chan, A review of anode materials development in solid oxide fuel cells, Journal of Materials Science 39 (2004) 4405–4439.
[3] A.L. Sauvet, J. Fouletier, Catalytic properties of new anode materials for solid oxide fuel cells operated under methane at intermediary temperature, Journal of Power Sources 101 (2001) 259–266.
[4] T. Takeguchi, Y. Kani, T. Yano, R. Kikuchi, K. Eguchi, K. Tsujimoto, Y. Uchida, A. Ueno, K. Omoshiki, M. Aizawa, Study on steam reforming of CH_4 and C_2 hydrocarbons and carbon deposition on Ni-YSZ cermets, Journal of Power Sources 112 (2002) 588–595.
[5] A.L. Dicks, Hydrogen generation from natural gas for the fuel cell systems of tomorrow, Journal of Power Sources 61 (1996) 113–124.
[6] P. Azadi, R. Farnood, E. Meier, Preparation of multiwalled carbon nanotube-supported nickel catalysts using incipient wetness method,, Journal of Physical Chemistry A 114 (2010) 3962–3968.
[7] J. Jia, Y. Wang, E. Tanabe, T. Shishido, K. Takehira, Carbon fibers prepared by pyrolysis of methane over Ni/MCM-41 catalyst, Microporous and Mesoporous Materials 57 (2003) 283–289.
[8] O.A. Marina, N.L. Canfield, J.W. Stevenson, Thermal, electrical, and electrocatalytical properties of lanthanum-doped strontium titanate, Solid State Ionics 149 (2002) 21–28.
[9] P. Holtappels, J. Bradley, J.T.S. Irvine, A. Kaiser, M. Mogensen, Electrochemical characterization of ceramic SOFC anodes, Journal of the Electrochemical Society 148 (2001) A923–A929.

[10] W.Z. Zhu, S.C. Deevi, A review on the status of anode materials for solid oxide fuel cells, Materials Science and Engineering A 362 (2003) 228–239.
[11] M. Itome, A.E. Nelson, Methane oxidation over M–8YSZ and M–CeO_2/8YSZ (M = Ni, Cu, Co, Ag) catalysts, Catalysis Letters 106 (2006) 21–27.
[12] R.J. Gorte, S. Park, J.M. Vohs, C. Wang, Anodes for direct oxidation of dry hydrocarbons in a solid-oxide fuel cell, Advanced Materials 12 (2000) 1465–1469.
[13] A. Trovarelli, Catalytic properties of ceria and CeO_2-containing materials, Catalysis Reviews 38 (1996) 439–520.
[14] D.B. Ingram, S. Lunic, First-principles analysis of the activity of transition and noble metals in the direct utilization of hydrocarbon fuels at solid oxide fuel cell operating conditions, Journal of the Electrochemical Society 156 (2009) B1457–B1465.
[15] T. Ishihara, J. Yan, M. Shinagawa, H. Matsumoto, Ni–Fe bimetallic anode as an active anode for intermediate temperature SOFC using $LaGaO_3$ based electrolyte film, Electrochimica Acta 52 (2006) 1645–1650.
[16] B. Huang, S.R. Wang, R.Z. Liu, T.L. Wen, Preparation and performance characterization of the Fe–Ni/ScSZ cermet anode for oxidation of ethanol fuel in SOFCs, Journal of Power Sources 167 (2007) 288–294.
[17] H. Kan, H. Lee, Enhanced stability of Ni–Fe/GDC solid oxide fuel cell anodes for dry methane fuel, Catalysis Communications 12 (2010) 36–39.
[18] J.A. Dean, in: Lange's Handbook of Chemistry, 15th ed., McGraw-Hill Inc., New York, 1999, pp. 4.31–4.32.
[19] J. Zielinski, I. Zglinicka, Z. Kaszkur, Reduction of Fe_2O_3 with hydrogen, Applied Catalysis A: General 381 (2010) 191–196.
[20] M. Bahgat, M.H Khedr, M.I. Nasr, E.K. Sedeek, Effect of firing temperature and reducing gas composition during low-temperature reduction of nanocrystalline Fe_2O_3, Metallurgical and Materials Transactions B: Process Metallurgy and Materials Processing Science 38B (2007) 5–11.
[21] R. Balachandran, H.K. Yow, B.H. Ong, K.B. Tan, K. Anuar, H.Y. Wong, Surface morphology and electrical properties of pulse electrodeposition of NiFe films on copper substrates in ultrasonic field, International Journal of Electrochemical Science 6 (2011) 3564–3579.
[22] N.V. Myung, D.Y. Park, B.Y. Yoo, P.T.A. Sumodjo, Development of electroplated magnetic materials for MEMS, Journal of Magnetism and Magnetic Materials 265 (2003) 189–198.
[23] C.Y. Ho, M.W. Ackerman, K.Y. Wu, T.N. Havill, R.H. Bogaard, R.A. Matula, S.G. Oh, H.M. James, Electrical resistivity of ten selected binary alloy systems, Journal of Physical and Chemical Reference Data 12 (1983) 183–323.
[24] S.L.Cheng, Z.H. Kuo, C.H. Chung, Structural and electrical properties of Ni and Ni–Co nanowires synthesized by electrodeposition in anodic alumina templates, Proceedings Nanoelectronic Conference (INEC), IEEE 4th International, pp. 1–2, Tao-Yuan, Taiwan (2011).
[25] D. Duprez, M.C. Demicheli, P. Marecot, J. Barbier, O. Ferretti, E.N. Ponzi, Deactivation of steam-reforming model catalysts by coke formation: I. Kinetics of the formation of filamentous carbon in the hydrogenolysis of cyclopentane on Ni/Al_2O_3 catalysts, Journal of Catalysis 124 (1990) 324–335.
[26] C.H. Bartholomew, Carbon deposition in steam reforming and methanation, Catalysis Reviews - Science and Engineering 24 (1982) 67–112.
[27] E. Nikolla, J. Schwank, S. Linic, Promotion of the long-term stability of reforming Ni catalysts by surface alloying, Journal of Catalysis 250 (2007) 85–93.